Received: 14 November 2019 | Revised: 17 March 2020 | Accepted: 8 April 2020

DOI: 10.1096/fj.201902888R

RESEARCH ARTICLE

THE FASEB JOURNAL

Fibronectin rescues aberrant phenotype of endothelial cells lacking either CCM1, CCM2 or CCM3

Konrad Schwefel[1,2] | Stefanie Spiegler[1,2] | Bettina C. Kirchmaier[3,4] | Patricia K. E. Dellweg[1,2] | Christiane D. Much[1,2] | Jan Pané-Farré[5] | Tim M. Strom[6,7] | Katharina Riedel[5] | Ute Felbor[1,2] | Matthias Rath[1,2]

[1]Department of Human Genetics, University Medicine Greifswald, Greifswald, Germany

[2]Interfaculty Institute of Genetics and Functional Genomics, University of Greifswald, Greifswald, Germany

[3]Institute of Cell Biology and Neuroscience, University of Frankfurt, Frankfurt am Main, Germany

[4]Buchmann Institute for Molecular Life Sciences, University of Frankfurt, Frankfurt am Main, Germany

[5]Department of Microbial Physiology and Molecular Biology, Institute of Microbiology, University of Greifswald, Greifswald, Germany

[6]Institute of Human Genetics, Technische Universität München, Munich, Germany

[7]Institute of Human Genetics, Helmholtz Zentrum München, Neuherberg, Germany

Correspondence
Matthias Rath, Department of Human Genetics, University Medicine Greifswald, Fleischmannstraße 43, Greifswald D-17475, Germany.
Email: matthias.rath@med.uni-greifswald.de

Present address
Jan Pané-Farré, Center for synthetic Microbiology (SYNMIKRO) and Department of Chemistry, Philipps University Marburg, Marburg, Germany

Funding information
Deutsche Forschungsgemeinschaft (DFG), Grant/Award Number: DFG RA2876/2-2; Research Network Molecular Medicine of the University Medicine Greifswald, Grant/Award Number: FOVB-2019-01; Gerhard Domagk program of the University Medicine Greifswald

Abstract

Loss-of-function variants in *CCM1/KRIT1*, *CCM2*, and *CCM3/PDCD10* are associated with autosomal dominant cerebral cavernous malformations (CCMs). CRISPR/Cas9-mediated CCM3 inactivation in human endothelial cells (ECs) has been shown to induce profound defects in cell-cell interaction as well as actin cytoskeleton organization. We here show that CCM3 inactivation impairs fibronectin expression and consequently leads to reduced fibers in the extracellular matrix. Despite the complexity and high molecular weight of fibronectin fibrils, our in vitro model allowed us to reveal that fibronectin supplementation restored aberrant spheroid formation as well as altered EC morphology, and suppressed actin stress fiber formation. Yet, fibronectin replacement neither enhanced the stability of tube-like structures nor inhibited the survival advantage of $CCM3^{-/-}$ ECs. Importantly, CRISPR/Cas9-mediated introduction of biallelic loss-of-function variants into either *CCM1* or *CCM2* demonstrated that the impaired production of a functional fibronectin matrix is a common feature of CCM1-, CCM2-, and CCM3-deficient ECs.

KEYWORDS

cerebral cavernous malformations, CRISPR/Cas9 genome editing, extracellular matrix

Abbreviations: CCM, cerebral cavernous malformation; CI-huVECs, immortalized human umbilical vein endothelial cells from InSCREENeX; DOC, deoxycholate; EC, endothelial cell; ECM, extracellular matrix; EDA, extra domain A; EDB, extra domain B; FAK, focal adhesion kinase; FC, fold change; FDR, false discovery rate; RNP, ribonucleoprotein.

1 | INTRODUCTION

Cerebral cavernous malformations (CCMs) belong to the most common cerebrovascular lesions and can be found in the brain and spinal cord. They are characterized by tightly packed convolutes of low-flow leaky vessels that are lined by a single layer of endothelial cells (ECs), lack supporting elastic fibers or vascular smooth muscle cells in their walls, and tend to bleed into the surrounding brain tissue.[1-4] CCM can occur in a sporadic or autosomal-dominant familial form (OMIM: 116860, 603284, 603285). The latter often presents with multiple CCMs at a younger age. Protein-truncating variants in either *CCM1* [also known as *KRIT1*[5,6]], *CCM2* [*MGC4607*, *OSM*[7,8]], or *CCM3* [*PDCD10*, *TFAR15*[9]] can be identified in up to 98% of familial CCM patients.[10,11] The CCM proteins act together in a heterotrimeric complex but also independently in different signaling pathways.[12] Recent in vitro and in vivo studies have given fascinating new insight into CCM pathobiology and their findings may help to identify a pharmacological approach for CCM management.[13-20]

EC proliferation, migration, morphogenesis, survival, and vascular stability depend on cell adhesion to the extracellular matrix (ECM), which is a scaffold for vascular organization and acts by transmitting mechanical forces.[21] Binding of ECM proteins to integrins can regulate a complex network of intracellular signaling pathways. However, it is not yet fully understood to what extent ECM components contribute to endothelial function and angiogenesis as they can have overlapping functions.[22-24] Notably, EC morphogenesis depends on stabilization by laminin-rich matrices but also on activation by collagen- or fibronectin-rich matrices.[25-27] Since less expression and irregular distribution of the major ECM component fibronectin have been observed in CCM lesions,[28] it is reasonable to hypothesize that the ECM plays an important role in CCM formation. It has also been demonstrated that CCM proteins regulate cell-matrix signaling,[29,30] cytoskeletal reorganization,[31-33] and stabilization of cell-cell junctions.[34,35]

In the present study, we demonstrate that loss of CCM1, CCM2, and CCM3 in human ECs impairs the production of a functional fibronectin matrix, which might trigger CCM formation. We also show that fibronectin replacement suppresses actin stress fiber formation and rescues endothelial dysfunctions of CCM1-, CCM2-, and CCM3-deficient ECs. In particular, a 120 kD cell-binding fragment of fibronectin is critical to restore spheroid formation, cortical actin organization, and EC morphology.

2 | MATERIALS AND METHODS

2.1 | Cell culture

Immortalized human umbilical vein ECs (CI-huVECs, InSCREENeX, Braunschweig, Germany) and human cerebral microvascular ECs (hCMEC/D3; Merck Millipore, Darmstadt, Germany) were cultured at 37°C and 5% of CO_2 in EC growth medium (ECGM, PromoCell, Heidelberg, Germany) supplemented with 10% of fetal calf serum (FCS, Thermo Fisher Scientific, Waltham, MA, USA) or in EndoGRO-MV complete medium (Merck Millipore) supplemented with 1 ng/mL of FGF-2 (PromoCell) and 5% of FCS, respectively. For rescue experiments, human plasma fibronectin (F2006, Sigma-Aldrich, St. Louis, MO, USA), human cellular fibronectin (F2518, Sigma-Aldrich), a proteolytic human plasma fibronectin 70 kD fragment (F0287, Sigma-Aldrich), a human fibronectin 120 kD cell attachment fragment (Part Number 175, YO Proteins, Ronninge, Sweden), human type IV collagen (C5533, Sigma-Aldrich), recombinant periostin (rPOSTN; RPH339Hu01, Cloud-Clone Corp., Katy, TX, USA), and recombinant fibulin-5 (rFBLN5; 9006-FB-050, R&D Systems, Minneapolis, MN, USA) were either supplemented to the ECGM or used to coat cell culture plates with the indicated concentrations. If not stated otherwise, the cells were cultured for 48 hours with ECM protein supplementation. Cells cultured on uncoated, tissue culture treated plates served as controls.

2.2 | CRISPR/Cas9 genome editing

Following our established protocol,[20] crRNA:tracrRNA:Cas9 ribonucleoprotein (RNP)-mediated genome editing was used to inactivate *CCM1*, *CCM2* or *CCM3*, respectively. In addition to the pre-identified CRISPR/Cas9 target region in *CCM3* exon 3 [LRG_651; 5′-CCT-GTGTTTAATGAGGTGAGTTG-3′; crRNA *CCM3*], target sequences located in *CCM1* exon 10 [LRG_650; 5′-CCA-TACTTTGGTCTAGGAGCTCC-3′; crRNA *CCM1*], and *CCM2* exon 4 [LRG_664; 5′-GGTC AGTTAACGTCCATACC-AGG-3′; crRNA *CCM2*] were selected using the Alt-R crRNA design tool (Integrated DNA Technologies, Leuven, Belgium). CI-huVECs and hCMEC/D3 cells were transfected with crRNA:tracrRNA:Cas9 RNP-complexes and clonally expanded as described before.[20] CCTop-CRISPR/Cas9 target online predictor[36] was used to identify potential off-target sides. The following criteria were used: (1) ≤ 4 crRNA mismatches and (2) ≤ 2 crRNA mismatches in the core of the first twelve nucleotides next to the PAM. Two exonic off-target regions were selected for each crRNA. T7EI assay was used to analyze off-target sides in crRNA:tracrRNA:Cas9 RNP-treated cell mixtures [off-target *CCM1*: 5′-CCA-TAC**C**TTGGTCT**C**GG**T**GC**G**CC-3′ (*ARVCF*), 5′-CCT-**G**AC**C**TTGGTCTA**A**GAGC**C**CC-3′ (*RNF44*); off-target *CCM2*: 5′-GG**AA**AGTTAA**A**GT**A**CA TACC-AGG-3′ (*PAPSS2*), 5′-G**A**TCAG**C**TAACGTC**A** AT**G**CC-TGG-3′ (*KDM4D*)]. Sanger sequencing was used to screen for off-target mutations in clonally expanded *CCM3*$^{-/-}$ cells [off-target *CCM3*: 5′-CCG-GTGTTTAATG AGGTGA**C**A**G**C-3' (*ZNF256*), 5′-CCT-GTGTTTAATGA

GACTAGATG-3′ (*ZNF586*)]. PCR primers used to amplify the CRISPR/Cas9 target and predicted off-target regions for Sanger sequencing or T7EI assays were as follows: *CCM1*: forward: 5′-ACAAGAGAAACTGCAAGGGTGA-3′, reverse: 5′-AATCCATACTTTGGTCTAGGAGC-3′; *CCM2*: forward: 5′-AGCCCTTGGTCCCTGTACTC-3′, reverse: 5′-GACAAACAGCAGCACCCAAC-3′; *CCM3*: forward: 5′-TGCTTTGTGAAGTAGTACCTAACCAAGGACT-3′, reverse: 5′-CTTCATAGTACTTCATCACCATTGTTCATTC-3′; *ARVCF*: forward: 5′-GCCTGAGGAGACCTGAGATG-3′, reverse: 5′- TGAGGTAGGCTCGAGAGAGT-3′; *RNF44*: forward: 5′-AGCACTCTCTTTCAGGCACC-3′, reverse: 5′-GCGCAAAAGAGTAGGAAGCG-3′; *PAPSS2*: forward: 5′-AGGATGTTCTAGGGCAGTTTGC-3′, reverse: 5′-GAGGACCAACAGTCATTGGAAG-3′; *KDM4D*: forward: 5′-TTTCAGCTCACAACCATACAC-3′, reverse: 5′-GCACAGTTGGCCTTAGACTTC-3′; *ZNF256*: forward: 5′-CCGAAGAATTCACACTGGAGTAA-3′, reverse: 5′-TCCTGTGTGAACTCTCTCATGTA-3′; *ZNF586*: forward: 5′-TTCACCAAAAGCCTACACTCCA-3′, reverse: 5′-GAACTCTCTGATGGCGACGG-3′. crRNA:tracrRNA: Cas9 RNP-treated cell mixtures and clonally expanded knockout CI-huVECs were used for functional assays in passage 25 or 28-31, respectively. hCMEC/D3 cells were used in passage 38-40.

2.3 | T7EI cleavage assay and amplicon deep sequencing

T7EI analyzes were performed as described before.[20] To analyze the CRISPR/Cas9-induced mutational spectrum, amplicon deep sequencing libraries were prepared with a custom two-step PCR approach following our established protocol.[20] PCR products were pooled and purified with Agencourt AMPure XP beads (Beckman Coulter, Pasadena, USA). The library was sequenced on a MiSeq instrument with 2 × 150 cycles (Illumina, San Diego, USA). The SeqNext software was used for data analysis (JSI Medical Systems, Ettenheim, Germany). Only variants with combined read frequencies ≥ 1% and quality score ≥ 25 were called. The following primers with adapter sequences were used for specific target enrichment: *CCM1*: forward: 5′-**ATCGGGAAGCTGAAG**AGCAATGTGGAGTAAAACCGA-3′, reverse: 5′-**ATCCGACGGTAGTGT**GATGACAAAGCTCTTAATGGGT-3′; *CCM2*: forward: 5′-**ATCGGGAAGCTGAAG**CTGGTGGCCTGAGTATGAAGC-3′, reverse: 5′-**ATCCGACGGTAGTGT**AGGATAGGGTTACCTTTGCATTG-3′; *CCM3*: forward: 5′-**ATCGGGAAGCTGAAG**TTGTGTCCAATTCTTTTATCACCA-3′, reverse: 5′-**ATCCGACGGTAGTGT**AGCAGGAATTAAAGAATTGCAGAGT-3′. In the second step, barcoded reverse primers and a universal forward primer were used to generate the final sequencing library.

2.4 | RNA isolation, RNA sequencing, and qPCR

The PeqGold TriFast reagent (Peqlab-VWR, Radnor, PA, USA) and Direct-zol RNA MiniPrep Plus Kit (Zymo Research, Irvine, CA, USA) were used to extract and purify total RNA. The integrity of the RNA samples was checked on a 2100 Bioanalyzer using the Agilent RNA 6000 Nano Kit (Agilent, Santa Clara, CA, USA). RNA concentrations were measured on a Qubit 2.0 (Thermo Fisher Scientific) with the Qubit RNA HS Assay Kit (Q32852, Thermo Fisher Scientific). Sequencing libraries were prepared with the TruSeq Stranded mRNA Kit according to the manufacturer's instructions (Illumina, San Diego, CA, USA). Pooled libraries were sequenced as 100 bp or 150 bp paired-end runs on a HiSeq 4000 instrument (Illumina). Reads that mapped to annotated genes were quantified with HTseq-count[37] and the Relative Log Expression (RLE) normalization, which is implemented in the R Bioconductor package DESeq2[38] was used to normalize gene counts. RNA sequencing data were uploaded to the Gene Expression Omnibus (GEO) database (record number: GSE138431). Transcripts with a $|\log_2 FC| > 2$ and $P_{adj} < .05$ were subjected to a PANTHER overrepresentation test (version 13.0; http://pantherdb.org/). The PANTHER GO-Slim Cellular Component annotation data set was used as reference list. The First Strand cDNA Synthesis Kit (Thermo Fisher Scientific) was used to transcribe mRNA into cDNA. Deregulated gene expressions of *FN1*, *POSTN,* and *FBLN5* were validated by SYBR Green-based qPCR on a Roche Light Cycler 480 instrument (Roche, Mannheim, Germany). The housekeeping gene *RPLP0* (ribosomal protein lateral stalk subunit P0) was used as an endogenous control. For detection of *FN1*, *POSTN,* and *FBLN5*, PrimeTime qPCR Primers were purchased from Integrated DNA Technologies (Hs.PT.58.40005963, Hs.PT.58.4452022, Hs.PT.58.14576443). The following primer pair were used for *RPLP0* qPCR: 5′-TCGACAATGGCAGCATCTAC-3′ and 5′-ATCCGTCTCCACAGACAAGG-3′.

2.5 | Western blot analyzes

Proteins were extracted with PeqGold TriFast reagent (Peqlab-VWR) and solubilized in buffer containing 8 M of Urea, 2 M of Thio-Urea, and 20 mM of Tris for CCM3 immunoblotting. Proteins of cell culture supernatant were precipitated with 20% of trichloroacetic acid and washed two times with ethanol before solubilization in buffer containing 8 M of Urea, 2 M of Thio-Urea, and 20 mM of Tris. For deoxycholate (DOC) assays, cells were treated as described before.[39] In brief, 200 000 cells were cultured on a 6-well plate, washed with phosphate-buffered saline (PBS, PromoCell), lysed with 500 µL of DOC buffer [2% of DOC, 20 mM of Tris-HCl (pH 8.8), 2 mM of

EDTA, 1× Halt protease and phosphatase inhibitor cocktail (Thermo Fisher Scientific)] and scraped from the cell culture plate. After centrifugation, the insoluble fraction was solubilized in SDS buffer [1% of SDS, 25 mM of Tris-HCl (pH 8.2), 2 mM of EDTA, 1× Halt protease, and phosphatase inhibitor cocktail]. Quantification was performed with the Qubit Protein Assay Kit (Thermo Fisher Scientific) on a Qubit 4 Fluorometer (Thermo Fisher Scientific) or with the Micro BCA Protein Assay Kit (Thermo Fisher Scientific). About 10 or 20 µg total protein were separated on 7.5% or 10% of TGX stain-free gels (Bio-Rad, Hercules, California, USA), transferred to PVDF membranes (Roche, Basel, Switzerland), immunostained with monoclonal mouse anti-human fibronectin (1:5000, MAB19182, R&D systems) or rabbit anti-CCM3 (1:150; IG-626, ImmunoGlobe, Himmelstadt, Germany), HRP conjugated mouse IgGκ light chain binding protein (1:30 000, sc-516102, Santa Cruz Biotechnology, Dallas, Texas, USA) or anti-rabbit HRP secondary antibody (1:30 000, sc-2357, Santa Cruz Biotechnology), Precision Protein StrepTactin-HRP Conjugate (1:15 000, Bio-Rad) and detected with Clarity Western ECL (Bio-Rad). A ChemiDoc XRS+ (Bio-Rad) imager was used for blot documentation of Stain-Free total protein and chemiluminometric signal detection. To semi-quantify relative CCM3 and fibronectin protein expression, normalized band intensities were calculated with the ImageLab software (v6.0, Bio-Rad). Since total protein can be used as reliable loading control,[40,41] the volume intensities of the detected protein bands were normalized to the volume intensities of the total protein fraction. For normalization of the DOC-insoluble fractions, total protein volume intensities of the DOC-soluble fractions were used. For relative fibronectin quantification in cell culture supernatants, the volume intensities of the detected protein bands were normalized to the cell number per 0.5 × 0.5 mm growth area, which was documented right before sample preparation.

2.6 | Phospho-kinase detection assay and immunofluorescence imaging

Relative phosphorylation levels of different human protein kinases were determined using the Proteome Profiler Human Phospho-Kinase Array Kit (ARY003B, R&D Systems) according to the manufacturer's instructions. In detail, approximately 1×10^7 cells/mL were solubilized in lysis buffer, and the total protein concentration was measured with the Qubit Protein Assay Kit (Thermo Fisher Scientific). About 600 µg were used per array set (A + B). A ChemiDoc XRS+ (Bio-Rad) imager was used for documentation, and pixel densities were determined using ImageJ software. For immunofluorescence analysis, 1×10^4 cells/well were cultured on a 96-well plate followed by fixation, permeabilization, and immunostaining as described previously.[20] In brief, cells were fixated with 4% paraformaldehyde at room temperature, permeabilized with 0.1% of Triton X-100 for 15 min, and blocked with 2% of normal goat serum for 1 hour. DNA and F-actin were visualized with DAPI (D9542, Sigma-Aldrich) and iFluor 488-conjugated phalloidin (ab176753, Abcam, Cambridge, UK), respectively. To analyze actin stress fiber formation, at least 120 cells per replicate were manually counted. Cells with short F-actin bundles spanning the nucleus were counted as stress fiber-positive. For fibronectin staining, cells were fixed with ice-cold (−20°C) methanol for 10 minutes. Primary mouse anti-human fibronectin antibodies (1:160, MAB19182, R&D Systems) and Alexa Fluor 488-conjugated secondary goat anti-mouse IgG antibodies (1:200, A-11029, Life Technology, Carlsbad, CA, USA) were incubated at RT for 1 hour. After adding Ibidi Mounting Medium (Ibidi, Martinsried, Germany), image acquisition was performed for each sample of an experiment with the same settings.

2.7 | Cell morphology, spheroid, and tube formation assay

CI-huVECs were seeded with 1×10^4 cells per well on a 96-well plate that had been coated with fibronectin to study cell morphology. Uncoated, tissue culture treated plates served as controls. After 48 hours, at least 300 cells were manually counted to determine the proportion of cells with a compact morphology. Approximately 400 cells were cultured for 24 hours with or without ECM protein supplementation in methocel containing medium (2.4 g/L) as hanging drop (25 µL) to study spheroid formation. The ImageJ software was used to analyze the spheroid cross-sectional areas and circularities of at least 10 spheroids per replicate. In brief, we manually traced the perimeters of each individual spheroid in ImageJ, calculated the lengths of the perimeters (l) in pixels as well as the areas (A) of the selections in square pixels and finally converted the values into millimeters or square millimeters by spatial calibration of the images. The following equation was used to calculate the circularity of the spheroids: $\frac{4\pi A}{l^2}$. To analyze tube formation, 2×10^4 cells were cultured on Matrigel (Corning, Kaiserslautern, Germany) in 96-well plates or Angiogenesis µ-Slides (Ibidi). The number of master segments (number of tubes), total master segments length (tube length), and mesh numbers were quantified after 20 hours with the Angiogenesis Analyzer ImageJ plugin.[42] For these assays, bright-field monochrome images were acquired with the EVOS FL Cell Imaging System at 4× (AMEP4680) or 10× (AMEP4681) magnification.

2.8 | Caspase-3 activity and ECM cell adhesion assays

After 72 hours of fibronectin supplementation, CI-huVECs were incubated for 2 hours with 1 μM of staurosporine to induce apoptosis. The Caspase-3 DEVD-R110 Fluorometric HTS Assay Kit (Biotium, Fremont, CA, USA) was used according to the manufacturer's instructions.

The ability of $CCM3^{+/+}$ and $CCM3^{-/-}$ CI-huVECs to bind to fibronectin, type I collagen, type II collagen, type IV collagen, laminin, tenascin, and vitronectin was quantified with a fluorometric ECM Cell Adhesion Array Kit (ECM545, Sigma-Aldrich) according to the manufacturer's instructions. In brief, CI-huVECs were resuspended in assay buffer and seeded in precoated 96-well plates with 1.5×10^5 cells/well. After 2 hours at 37°C and 5% of CO_2, nonadherent cells were aspirated and the wells were washed three times with assay buffer. Finally, the sample wells were incubated for 15 minutes with a solution of 4X cell lysis buffer and CyQuant GR dye, which shows an enhancement of fluorescence when bound to cellular nucleic acids. Fluorescence intensity was measured in relative fluorescence units (RFU) at Ex/Em (nm) = 470/510-580. Bovine serum albumin coated wells served as control.

2.9 | Microscope image acquisition

An EVOS FL Cell Imaging System (Thermo Fisher Scientific; Sony ICX445 monochrome CCD; EVOS Light Cube DAPI, GFP, RFP; 10× AMEP4681, 40x AMEP4683) or a Zeiss LSM 510 META Confocal Microscope (Carl Zeiss AG, Oberkochen, Germany; Zeiss LSM Software 3.5 plus; meta detector; laser: 405 nm, 488 nm; major beam splitter: HFT 405/488/561 nm; band-pass filter: 505-550 nm; Plan-Neofluar 40×/1.3 Oil DIC) were used for image acquisition.

2.10 | Statistical analysis

GraphPad Prism software (v.8.0.1, GraphPad Software, LA Jolla, CA, USA) was used for data analyzes. Data are presented as mean and single data points if not stated otherwise. Two-tailed, Student's *t* tests, multiple *t* tests, and two-way ANOVA with Holm-Šidák's multiple comparisons tests were used for two or more groups, respectively. RNA sequencing data were analyzed with Wald test and the Benjamini-Hochberg procedure for multiple testing, while Fisher's Exact test with false discovery rate (FDR) multiple test correction was used for PANTHER overrepresentation analysis. *P*-values <.05 and *q*-values <.05 were regarded as statistically significant.

3 | RESULTS

We have recently demonstrated that CRISPR/Cas9-induced CCM3 inactivation in human ECs induces profound morphological and functional changes.[20] In our present study, we used genome-wide RNA sequencing of $CCM3^{+/+}$ and $CCM3^{-/-}$ CI-huVECs to get a better understanding of the underlying molecular mechanisms. About 569 upregulated or downregulated genes ($|\log_2 FC| > 2$ and $p_{adj} < .05$) were identified in clonally expanded CCM3-deficient ECs (Figure 1A,B). A gene set enrichment analysis revealed an overrepresentation of cell junction, extracellular region, and plasma membrane components (Table 1).

We focused our further analyzes on *FN1* ($\log_2 FC = -2.3$; $p_{adj} = 2.10 \times 10^{-99}$), *POSTN* ($\log_2 FC = -8.5$; $p_{adj} = 2.68 \times 10^{-226}$), and *FBLN5* ($\log_2 FC = -8.2$; $p_{adj} = 2.44 \times 10^{-197}$) since they were either the most downregulated genes in $CCM3^{-/-}$ CI-huVECs (*POSTN* and *FBLN5*) or highly expressed in wild-type $CCM3^{+/+}$ but significantly downregulated in $CCM3^{-/-}$ CI-huVECs (*FN1*). Expression differences of the three genes that encode for the ECM glycoprotein fibronectin or the matricellular proteins periostin and fibulin-5, respectively, were validated by RT-qPCR (Figure 1C). Fibronectin is important for proper ECM assembly[43] and the highest endothelial *FN1* expression has been found in the brain,[44] suggesting that it might support the integrity of the neurovascular unit. Therefore, we decided to study the role of fibronectin in CCM pathogenesis in more detail. In Western Blot analyzes, we observed less fibronectin in the cell culture supernatants of $CCM3^{-/-}$ CI-huVECs and reduced DOC-insoluble fibronectin aggregates upon CCM3-inactivation (Figure 1D). No fibronectin was detected in the DOC-soluble fractions.

To test whether $CCM3^{-/-}$ CI-huVECs have a cell-to-ECM adhesion defect, we used cell culture plates coated with fibronectin, type I, II, and IV collagens, laminin, tenascin, and vitronectin in a fluorometric cell adhesion array approach. Of note, binding of CCM3-deficient ECs to exogenous fibronectin was intact and no major cell binding abnormalities were observed for the other ECM components (Figure 1E). These results confirmed that long-term CCM3 inactivation impairs *FN1* expression but not the adhesion of CI-huVECs to fibronectin. This is consistent with the observation that supplementation of plasma fibronectin enhanced fibronectin fiber assembly in the ECM of $CCM3^{-/-}$ CI-huVECs (Figure 1F). Therefore, we next examined whether exogenous fibronectin supplementation could rescue the endothelial dysfunction of CCM3-deficient ECs.

3.1 | Fibronectin replacement improves spheroid formation and prevents actin stress fiber assembly

Fibronectin supplementation significantly attenuated the aberrant phenotype of $CCM3^{-/-}$ CI-huVECs. In particular, they

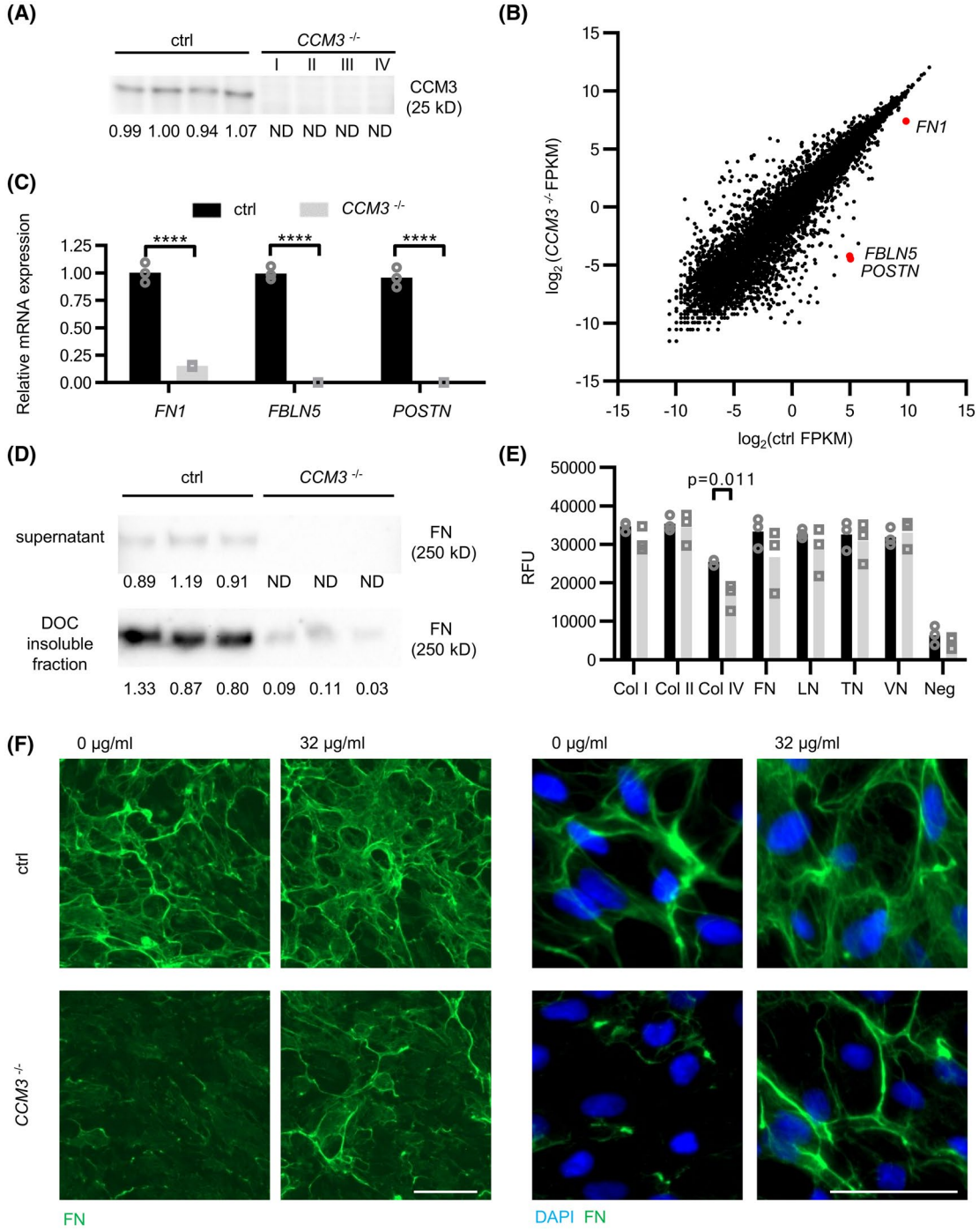

FIGURE 1 Deregulation of extracellular matrix components after long-term CCM3 inactivation. A, Western Blot analyzes verified complete CCM3 inactivation in clonally expanded *CCM3*$^{-/-}$ CI-huVECs used in this study (clones I-IV). Expression levels normalized to the *CCM3*$^{+/+}$ control group are given below the panel. B, RNA-Seq data of *CCM3*$^{+/+}$ control (*x*-axis) and *CCM3*$^{-/-}$ CI-huVECs (*y*-axis) are presented as scatter dot plot. FPKM = fragments per kilobase of exon model per million mapped reads. C, Expression levels of *FN1*, *FBLN5,* and *POSTN* were validated by qPCR. D, Western Blot results revealed less fibronectin in cell culture supernatants of *CCM3*$^{-/-}$ CI-huVECs and reduced DOC-insoluble fibronectin aggregates upon CCM3-inactivation. Expression levels normalized to the *CCM3*$^{+/+}$ control group are given below the subpanels. E, Fluorometric cell adhesion assays demonstrated no major cell binding abnormalities of *CCM3*$^{-/-}$ CI-huVECs to ECM components. F, A reduced fibronectin expression was observed in immunofluorescence imaging of 1×10^4 cells/well cultured on a tissue culture treated 96-well plate after 48 hours. Plasma fibronectin supplementation promoted fibronectin matrix assembly. Scale bars ≙ 100 µm in the left and 50 µm in the right panels. Images were acquired using the same setting for each sample and no changes were implemented. ND = not detected, RFU = relative fluorescence units, ctrl = *CCM3*$^{+/+}$ control cells, Col I = type I collagen, Col II = type II collagen, Col IV = type IV collagen, FN = fibronectin, LN = laminin, TN = tenascin, VN = vitronectin, and Neg = bovine serum albumin. Data are presented as mean and single data points (n = 3-4). Multiple *t* tests were used for statistical analyzes. ****$P < .0001$

TABLE 1 Gene set enrichment analysis

PANTHER GO-slim cellular component	# Genes	FC	FDR
Neuronal cell body	3	8.27	0.0479
Cell junction	10	4.44	0.0036
Extracellular region	30	1.88	0.0117
Integral to membrane	39	1.77	0.0098
Plasma membrane	56	1.64	0.0060
Membrane	43	1.55	0.0407
Intracellular	102	0.79	0.0421
Organelle	58	0.6	0.0004
Nucleus	24	0.5	0.0045
Mitochondrion	3	0.24	0.0239

Note: Over- and underrepresented terms in PANTHER cellular component analysis are marked in green and red, respectively.

Abbreviations: FC, fold change; FDR, false discovery rate.

lost their rounded morphology and recovered a spindle-like cell shape when cultured on plates, which had been coated with human plasma fibronectin (Figure 2A). Moreover, fibronectin replacement suppressed actin stress fiber formation and rescued the inability to form round and demarcated spheroids in 3D culture. When cultured in plasma fibronectin-containing hanging drops, the circularity of spheroids formed by *CCM3*$^{-/-}$ CI-huVECs increased significantly and their cross-sectional area decreased to nearly normal levels when compared to spheroids formed by *CCM3*$^{+/+}$ wild-type cells (Figure 2B). Besides, normalization of cortical actin filaments and less actin stress fibers were observed in *CCM3*$^{-/-}$ CI-huVECs that had been cultured on fibronectin-coated plates (Figure 2C; Figure S1). As expected, fibronectin supplementation had no adverse effects on *CCM3*$^{+/+}$ wild-type cells. In contrast to these positive effects on cell morphology, organization of the actin cytoskeleton and spheroid formation, fibronectin did not increase the stability of tube-like structures formed by *CCM3*$^{-/-}$ CI-huVECs on Matrigel (Figure 2D). Although this is an initial screening assay to study the formation of vessel-like tubular networks in vitro,[45] reduced mesh and tube numbers as well as tube length reflect the instability of endothelial cords that has been described for ECs before.[20,46,47] Furthermore, the resistance of *CCM3*$^{-/-}$ CI-huVECs to staurosporine-induced apoptotic cell death was not rescued by fibronectin supplementation (Figure 2E).

Fibronectin binds to heterodimeric integrin receptors, which link the extracellular glycoprotein to cytoskeletal adapter proteins and the actin-assembly machinery.[48] The phosphorylation dependent activation of the focal adhesion kinase (FAK), members of the Src family of tyrosine kinases, and downstream signaling pathways play a critical role in adhesion signaling but needs to be tightly regulated since overactivation can lead to endothelial dysfunctions, for example, hyperpermeability.[49,50] We, therefore, wanted to exclude constitutive overactivation in *CCM3*$^{-/-}$ CI-huVECs after fibronectin supplementation. Phosphorylation profiling after 48 hours of fibronectin supplementation demonstrated no adverse long-term effects on the activation levels of FAK or Src family members (Figure 2F, Table S1). Using RNA sequencing, we addressed two questions: (1) Can a wild-type-like gene expression profile be restored in *CCM3*$^{-/-}$ CI-huVECs by fibronectin supplementation (*CCM3*$^{+/+}$ FN- vs *CCM3*$^{-/-}$ FN+; (Figure 2G)? (2) What gene expression differences are induced in *CCM3*$^{-/-}$ CI-huVECs by fibronectin supplementation in general (*CCM3*$^{-/-}$ FN- vs *CCM3*$^{-/-}$ FN+; Figure 2H)? Data analysis demonstrated neither significant gene expression differences ($|\log2FC| > 2$ and $P_{adj} < .05$) in *CCM3*$^{-/-}$ CI-huVECs upon fibronectin supplementation nor a rescue of their aberrant gene expression profile (Figure 2G,H). For instance, overexpression of *KLF2*, which is known to induce actin shear fiber formation in ECs and has been described as key player in CCM pathogenesis,[14,17,51] was unaffected by fibronectin replacement (*CCM3*$^{-/-}$ FN+ vs *CCM3*$^{-/-}$ FN-, $\log_2FC = -0.19$, $P_{adj} = .25$ and *CCM3*$^{-/-}$ FN+ vs *CCM3*$^{+/+}$ FN-, $\log_2FC = 3.3$, $P_{adj} = 3.73 \times 10^{-139}$). In conclusion, our results demonstrate that the restoration of a fibronectin-rich matrix is sufficient to induce partial rescue of the aberrant phenotype of CCM3-deficient ECs. Similar fibronectin rescue effects were observed in clonally expanded *CCM3*$^{-/-}$ hCMEC/D3 cells (Figure 3).

3.2 | The cell-binding fragment of fibronectin is essential to rescue the altered endothelial phenotype

Plasma fibronectin exists as a soluble dimer of two covalently linked approx. 250 kD subunits with a complex structure of various functional domains. It differs from cellular fibronectin by the two extra domains A (EDA) and B (EDB). As verified by our RNA sequencing data, both isoforms are expressed by CI-huVECs (Figure S2). With two proteolytic plasma fibronectin fragments, we were able to narrow down the region that is crucial to suppress reorganization of the actin cytoskeleton to stress fibers and rescue the dysfunction of CCM3-deficient ECs. The 70 and 120 kD fragments, as well as the less-soluble cellular fibronectin isoform reduced actin stress fiber assembly in *CCM3*$^{-/-}$ CI-huVECs (Figure 4A) but only the 120 kD cell attachment fragment with its RGD domain and major integrin interaction sites also normalized spheroid formation (Figure 4B). The N-terminal 70 kD region of fibronectin does not only contain the assembly domain, but can also stimulate outside-in signaling.[52] Interestingly, it has already been demonstrated that the N-terminal 70 kD fragment can bind α5β1 integrins and control actin assembly.[53] This might be an explanation

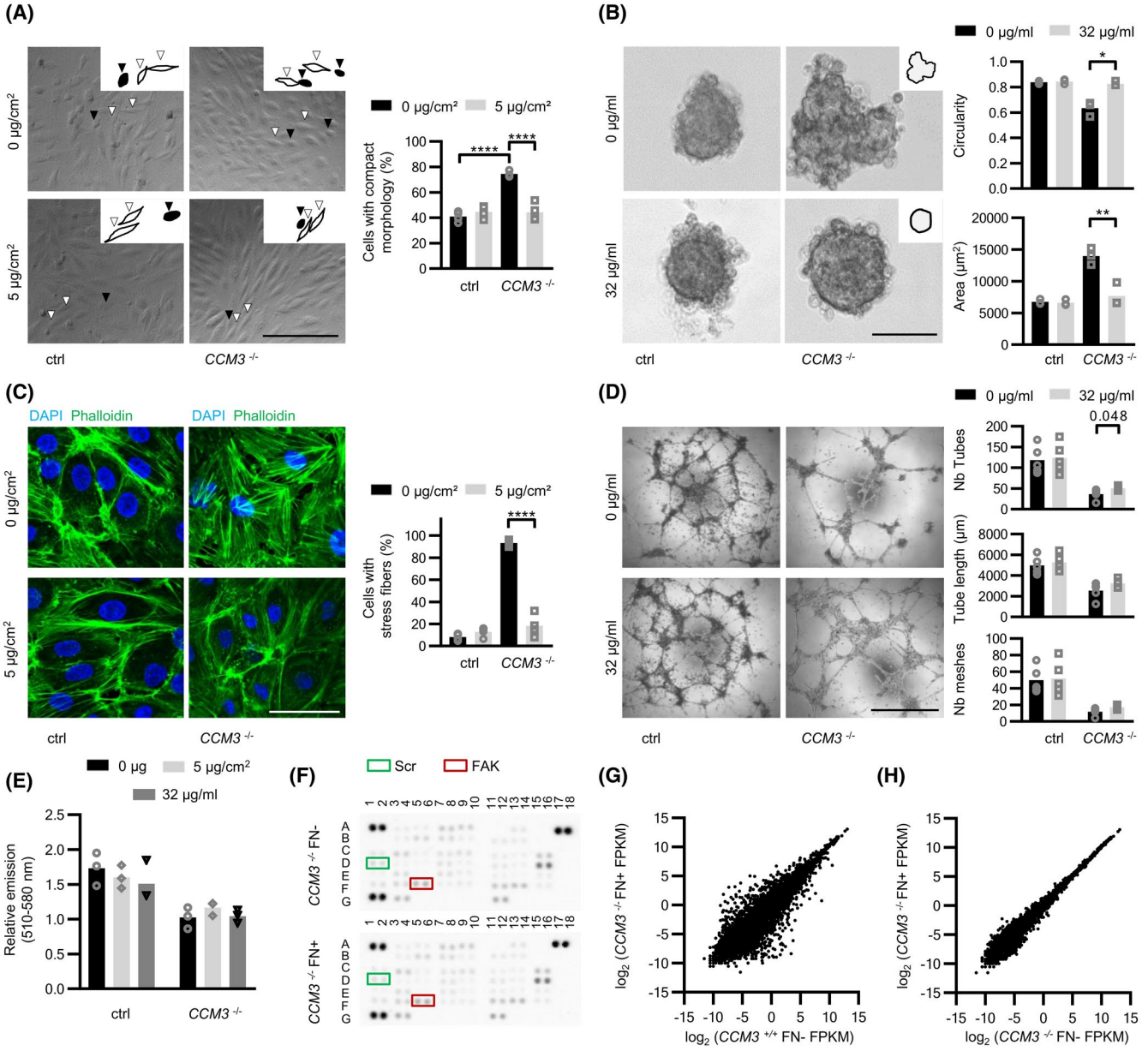

FIGURE 2 Restored endothelial function of *CCM3*$^{-/-}$ CI-huVECs by fibronectin replacement. A, *CCM3*$^{-/-}$ CI-huVECs cultured on fibronectin coated plates (5 µg/cm^2) regained a typical endothelial morphology. Black arrowheads indicate a compact cell shape, while white arrowheads indicate cells that show a spindle-shaped morphology. *CCM3*$^{+/+}$ and *CCM3*$^{-/-}$ CI-huVECs were seeded with 1×10^4 cells/well on a 96-well plate. Scale bar ≙ 200 µm. B, Fibronectin supplementation (32 µg/mL) significantly improved the spheroid organization of *CCM3*$^{-/-}$ CI-huVECs. The circularity and the cross-sectional area of the spheroids were determined. The manually traced perimeter of the shown spheroid is depicted in the upper right corner. Scale bar ≙ 100 µm. C, *CCM3*$^{-/-}$ CI-huVECs cultured on fibronectin-coated plates demonstrated a reduced actin stress fiber formation (1×10^4 cells/well; 96-well plate). Confocal microscopy was used for image acquisition. Phalloidin-iFluor 488 and DAPI staining are shown in green and blue, respectively. The brightness was adjusted equally for all images to show the relevant structures of F-actin formation. Original images are shown in Figure S1. Scale bar ≙ 50 µm. D, The reduced ability of *CCM3*$^{-/-}$ CI-huVECs to form tube-like structures could not be rescued by fibronectin supplementation (32 µg/mL). Scale bar ≙ 1 mm. E, Neither fibronectin coating (5 µg/cm^2) nor supplementation to the culture medium (32 µg/mL) had an effect on staurosporine-induced Caspase-3 activity. F, Representative Phospho-Kinase array membranes are shown for *CCM3*$^{-/-}$ CI-huVECs cultured without and with fibronectin supplementation (5 µg/cm^2). Spots showing the detection of phosphorylated forms of Src and FAK are marked in green or red, respectively. G and H, RNA-Seq data of *CCM3*$^{+/+}$ control cells without (*x*-axis) and *CCM3*$^{-/-}$ CI-huVECs with 5 µg/cm^2 fibronectin supplementation (*y*-axis) (G) or *CCM3*$^{-/-}$ CI-huVECs without (*x*-axis) and with (*y*-axis) fibronectin supplementation (H) are presented as scatter dot plot. FPKM = fragments per kilobase of exon model per million mapped reads. ctrl = *CCM3*$^{+/+}$ control cells, FN = fibronectin, Nb = Number. Data are presented as mean and single data points (n = 3-5). Two-way ANOVA with Holm-Šidák's multiple comparisons test, multiple *t* test or Student's *t* test were used for statistical analyzes: *$P < .05$; **$P < .01$; ****$P < .0001$

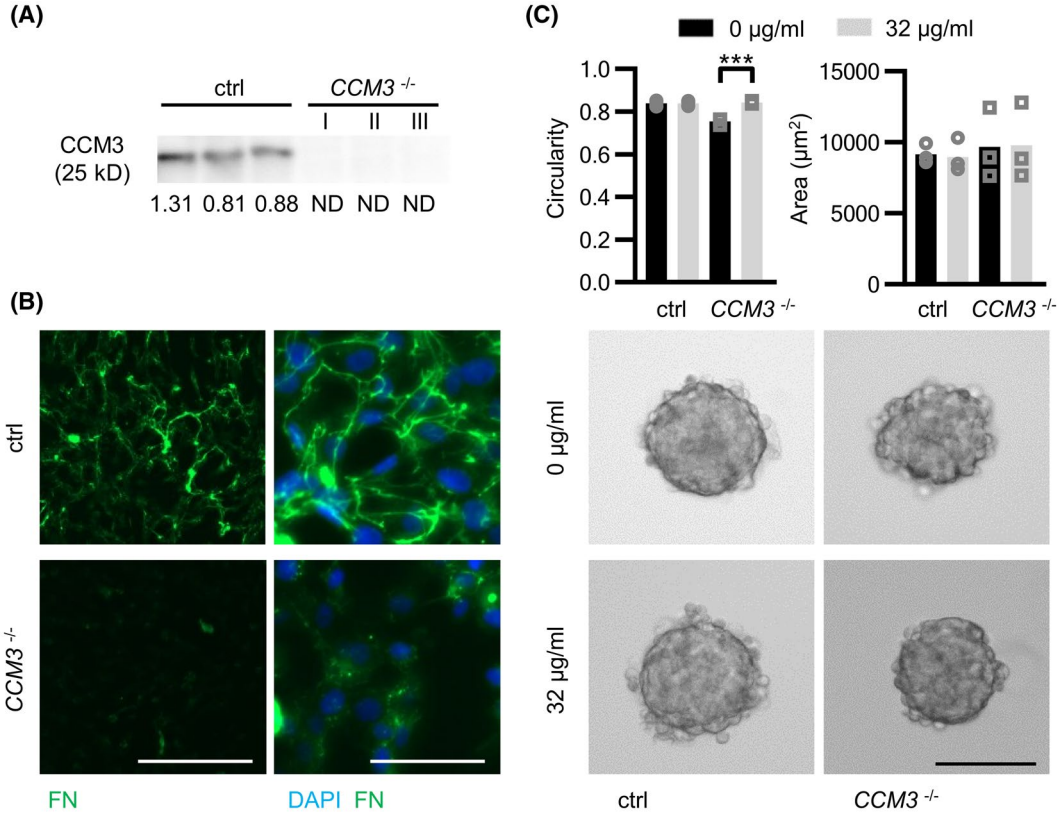

FIGURE 3 Fibronectin replacement improves spheroid organization of *CCM3*$^{-/-}$ hCMEC/D3 cells. A, Western Blot analyzes verified complete CCM3 inactivation in clonally expanded hCMEC/D3 used in this study (clones I-III). Expression levels normalized to the *CCM3*$^{+/+}$ control group are given below the panel. B, A reduced fibronectin expression was observed in immunofluorescence imaging of cells cultured on a tissue culture treated 96-well plate (1×10^4 cells/well). Scale bars ≙ 200 µm in the left and 50 µm in the right panels. C, Plasma fibronectin supplementation (32 µg/mL) significantly improved spheroid organization of *CCM3*$^{-/-}$ hCMEC/D3 cells. Shown are the circularity and the area of the spheroids. Scale bar ≙ 100 µm. ctrl = *CCM3*$^{+/+}$ hCMEC/D3 cells, FN = fibronectin, ND = not detected. Data are presented as mean and single data points (n = 3). Student's *t* test was used for statistical analyzes: ***$P < .001$

for the actin cytoskeleton reorganization that we observed in *CCM3*$^{-/-}$ CI-huVECs. However, the 70 kD fragment is also a well-known inhibitor of fibronectin matrix polymerization,[52,54] and therefore, might not be able to faciliate organization of spheroids formed by *CCM3*$^{-/-}$ CI-huVECs.

It is noteworthy to mention that supplementation of type IV collagen increased the circularity of *CCM3*$^{-/-}$ CI-huVEC spheroids but did not reduce actin stress fiber assembly (Figure 4A,B). Periostin replacement stabilized tube-like structures but did not attenuate dysfunctional cytoskeletal dynamics, and fibulin-5 treatment reduced stress fiber formation but induced severe morphological changes in *CCM3*$^{-/-}$ CI-huVECs (Figure 5).

3.3 | Dysregulation of the fibronectin matrix is a common feature of CCM1/2/3-deficiency

We next asked the question of whether inactivation of CCM1 and CCM2 in human ECs also impairs fibronectin expression. Thus, CRISPR/Cas9 genome editing was used for *CCM1* and *CCM2* gene disruption in CI-huVECs. Eight days after RNP-transfection, average T7EI cleavage efficiencies of 32% (n = 3; range: 31%-33%) and 17% (n = 3; range: 15%-19%) were observed, respectively. After thirteen days, these had increased to 43% (*CCM1*; range: 39%-48%) and 53% (*CCM2*; range: 47%-54%). These results are in line with the survival benefit of CCM3- and CCM1-deficient human ECs that we have described before.[20,55]

We could not identify commercial antibodies specific to CCM1 or CCM2 in this study. Nevertheless, the results of our deep sequencing analysis indicated protein inactivation in the vast majority of cells: A high proportion of *CCM1* and *CCM2* frameshift variants (71%-88%) was observed in cell mixtures that had been treated with *CCM1*- or *CCM2*-specific crRNA:tracrRNA:Cas9 RNPs, respectively (Figure 6). As expected, disruption of the *CCM1* and *CCM2* genes reduced fibronectin expression (Figure 6). Furthermore, supplementation of human plasma fibronectin rescued the impaired spheroid formation, the reorganization of the actin cytoskeleton, and the atypical rounded cell morphology that were observed in cell mixtures treated with *CCM1*- or

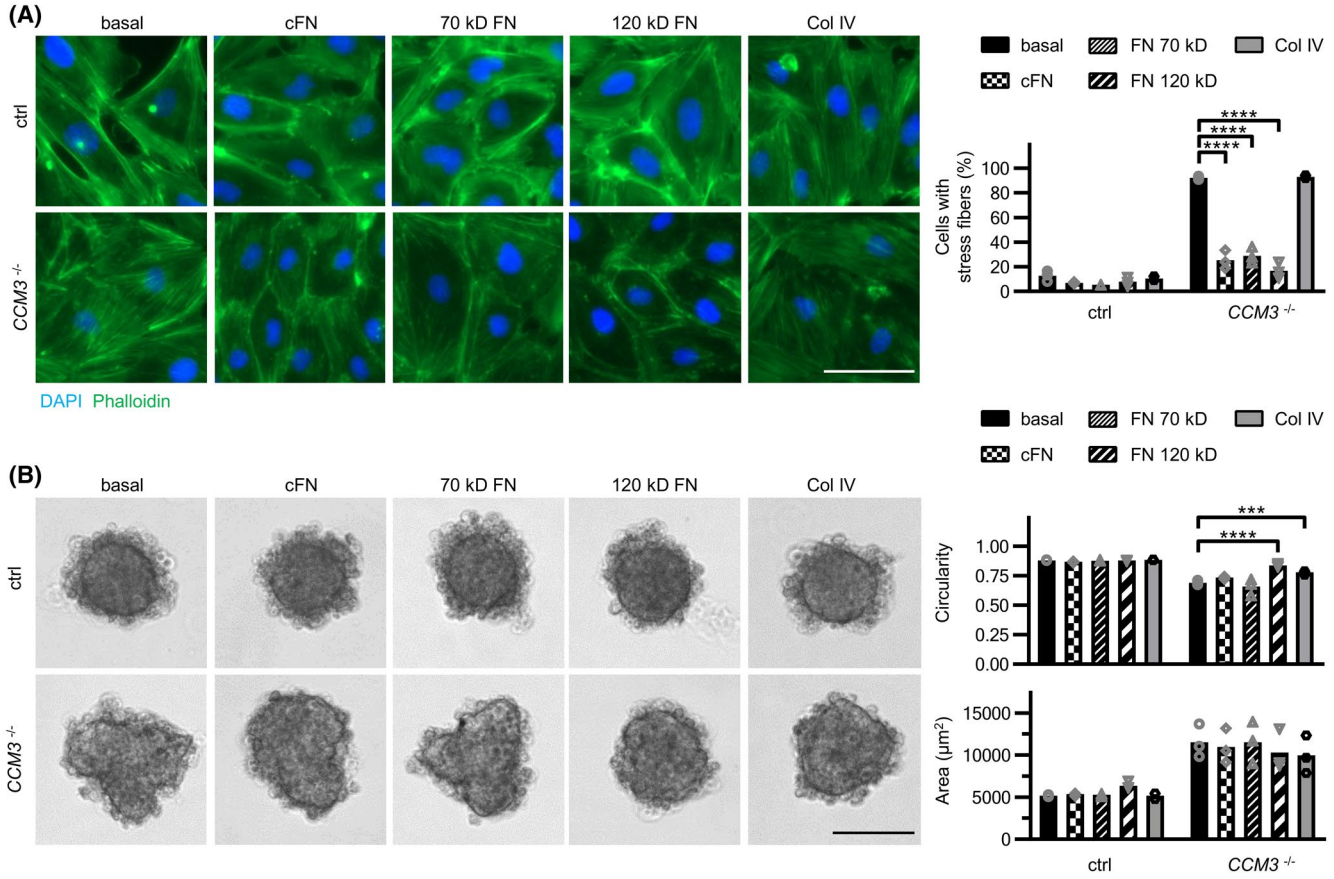

FIGURE 4 The 120 kD fragment of fibronectin is sufficient to rescue the cytoskeletal changes and spheroid organization of *CCM3*$^{-/-}$ CI-huVECs. A, Phalloidin-iFluor 488-(green) and DAPI-(blue) co-staining demonstrated that the actin stress fiber content was significantly decreased in *CCM3*$^{-/-}$ CI-huVECs that had been cultured on plates coated with cFN, 70 kD or 120 kD fibronectin fragments (5 µg/cm^2; 1×10^4 cells/well). Scale bar ≙ 50 µm. B, Only the supplementation of a 120 kD fibronectin fragment (32 µg/mL) and type IV collagen (60 µg/mL) but not of cellular fibronectin (cFN) or a 70 kD fibronectin fragment (32 µg/mL) significantly rescued circularity and proper spheroid organization of *CCM3*$^{-/-}$ CI-huVECs. Scale bar ≙ 100 µm. ctrl = *CCM3*$^{+/+}$ control cells, cFN = cellular fibronectin, 70 kD FN = 70 kD fibronectin fragment, 120 kD FN = 120 kD fibronectin fragment, Col IV = type IV collagen. Data are presented as mean and single data points (n = 3). Two-way ANOVA with Holm-Šidák's multiple comparisons test was used for statistical analyzes: ***$P < .001$, ****$P < .0001$

CCM2-specific crRNA:tracrRNA:Cas9 RNP-complexes, respectively (Figure 7). Together, these results indicate overlapping effects and regulation of endothelial fibronectin expression by CCM1, CCM2, and CCM3. In addition, alterations in potential off-target sites after crRNA:tracrRNA:Cas9 RNP-treatment targeting *CCM1*, *CCM2,* and *CCM3* could be excluded in all cell mixtures and clonal cell lines of CI-huVECs and hCMEC/D3 cells (Figure 6 and Data not shown).

4 | DISCUSSION

In this study, we show that CCM1, CCM2, and CCM3 regulate the production of a functional fibronectin matrix by human ECs. Our results also demonstrate that supplementation of fibronectin rescues morphological changes as well as impaired endothelial spheroid organization and normalizes actin stress fiber formation upon CRISPR/Cas9-induced inactivation of either CCM1, CCM2 or CCM3.

The formation of cavernous vascular malformations upon endothelial CCM3 inactivation has recently been associated with impaired dispersion of ECs in vivo.[56] The results of Castro and colleagues suggest that *CCM3*$^{-/-}$ ECs might be unable to build or remodel their ECM, which serves as a scaffold for coordinate migration. In addition to an important role in angiogenesis, the CCM proteins also contribute to the maintenance and regulation of the vascular endothelial barrier function.[57,58] Therefore, studying cytoskeletal remodeling, cell-cell, and cell-matrix interactions is useful to get a better understanding of the mechanisms leading to increased vascular permeability and recurrent bleeding events in CCM patients.

We here demonstrate that CRISPR/Cas9-induced *CCM3* gene disruption in ECs significantly impairs the expression of fibronectin in vitro. Our observation also reflects the situation in human CCM tissues, in which less and irregularly organized fibronectin fibrils have been noticed around CCM microvessels. Interestingly, this was accompanied by an altered dispersion of tight junction proteins.[28]

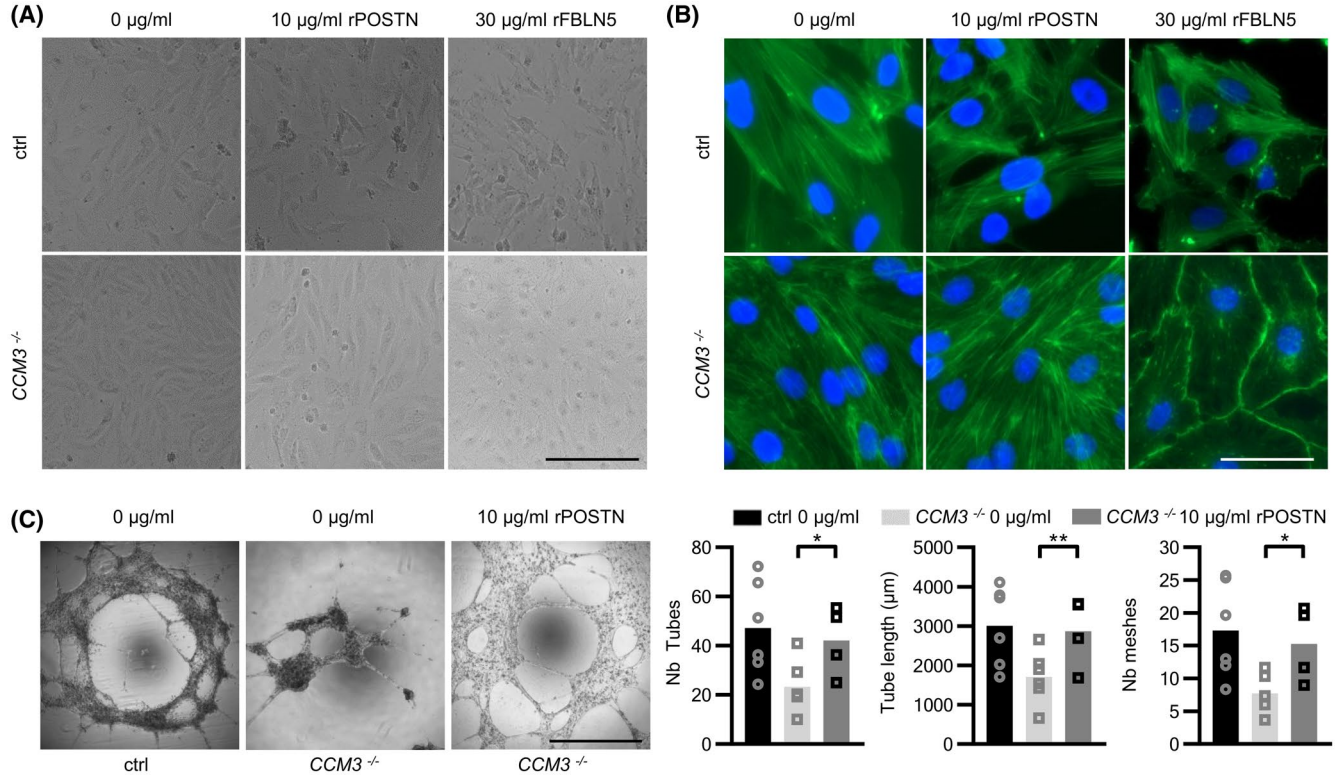

FIGURE 5 Supplemented periostin and fibulin-5 have different effects on *CCM3*$^{-/-}$ CI huVECs. A, Representative bright-field microscopy images and B, Phalloidin-iFluor 488 staining of F-actin indicated an altered cellular morphology and reduced stress fiber formation following supplementation of 30 µg/mL fibulin-5 to *CCM3*$^{-/-}$ CI-huVECs. Control cells and cells supplemented with 10 µg/mL periostin demonstrated no changes in cell morphology or F-actin organization (2×10^4 cells/well, 96-well plate). Scale bars ≙ 200 µm (A) and 50 µm (B). C, Replacement of periostin attenuated impaired tube formation after 20 hours in CCM3-deficient ECs. Shown are the tube length, the number (Nb) of tubes and the number of meshes. Scale bar ≙ 1 mm. ctrl = *CCM3*$^{+/+}$ control cells. Data are presented as mean and single data points (n = 3-6). Student's *t* test was used for statistical analyzes: **P* < .05, ***P* < .01

Besides, our study disclosed that the inability to produce a functional fibronectin matrix is not limited to CCM3 deficiency but is also a consequence of CCM1 and CCM2 inactivation in human ECs. CCM1, CCM2, and CCM3 are known to act together in the same signaling pathways but also independently from each other.[59-61] GST pull-down and co-immunoprecipitation studies have demonstrated that the three CCM proteins can form a ternary complex in vitro and that CCM2 acts as a linker molecule between CCM1 and CCM3.[62,63] The shared phenotype of CCM1-, CCM2-, and CCM3-deficient human ECs indicates that the three CCM proteins regulate the expression of fibronectin in a common pathway.

The formation of actin stress fibers has been consistently observed in CCM1-, CCM2-, and CCM3-deficient ECs.[20,33,64,65] Therefore, it has been widely used as surrogate marker for endothelial dysfunctions that are induced by CCM1/2/3 inactivation. Noteworthy, stress fiber formation was also a readout parameter in a recent pharmacological high-throughput screen and in one of the first studies that identified Rho kinase inhibition as a potential therapeutic approach in CCM disease.[31,66] Fibronectin directly participates in mechanosignaling and is linked to the cytoskeleton by the matrix-integrin-cytoskeletal signaling axis.[67,68] Its sustained binding to integrin receptors can induce RhoA activation and stress fiber assembly.[48] On the contrary, Rho-dependent cytoskeletal contractility also promotes fibronectin fibrillogenesis.[69] Therefore, reorganization of the actin cytoskeleton into stress fibers might be a compensatory mechanism to impaired fibronectin expression and lack of a fibronectin-rich ECM upon CCM protein inactivation. The paradoxical effect of fibronectin supplementation on *CCM1*$^{-/-}$, *CCM2*$^{-/-}$, and *CCM3*$^{-/-}$ CI-huVECs, namely suppression of actin stress fiber formation and restoration of the cortical actin network, supports this hypothesis. Notably, the formation of cortical actin filaments has been associated with enhanced endothelial barrier function[70] which would be beneficial in CCM pathogenesis.

Cseh and colleagues have demonstrated that supplementation of exogenous fibronectin can restore functional cell-cell junctions between fibronectin-depleted bovine ECs.[71] In addition, monolayers of porcine brain capillary

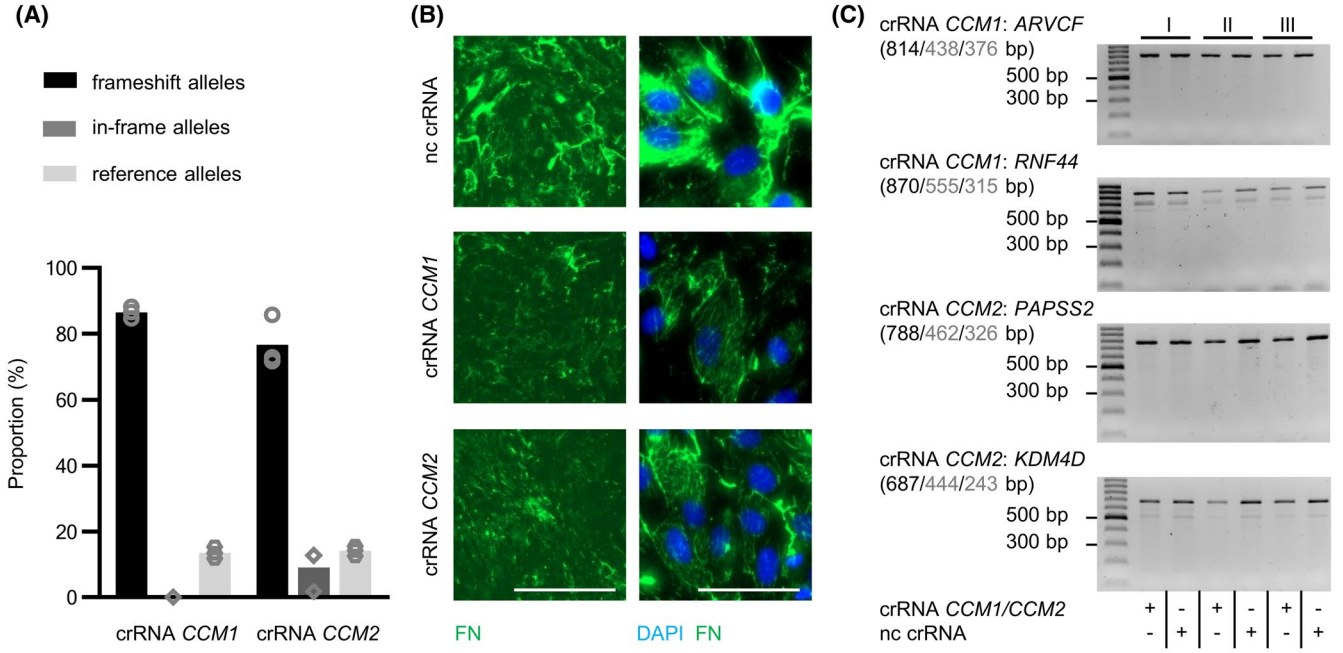

FIGURE 6 Deregulation of fibronectin expression upon CCM1 or CCM2 inactivation in CI-huVECs. A, High proportion of *CCM1* and *CCM2* loss-of-function alleles were found in crRNA:tracrRNA:Cas9 RNP-treated CI-huVEC mixtures. B, Immunofluorescence staining in crRNA:tracrRNA:Cas9 RNP-treated CI-huVECs indicated reduced fibronectin expression (1×10^4 cell/well, 96-well plate). Scale bars ≙ 200 µm in the left and 50 µm in the right panels. C, T7EI analyzes revealed no alterations in predicted off-target regions. Three independent replicates are shown (I-III). Expected length of uncleaved (black) and cleaved (gray) amplicons are depicted at the upper left of each subpanel. crRNA *CCM1* = *CCM1*-targeting RNP, crRNA *CCM2* = *CCM2*-targeting RNP, nc crRNA = non-targeting control RNP, FN = fibronectin. Data are presented as mean and single data points (n = 3)

ECs supplemented with fibronectin showed increased trans-endothelial electrical resistance (TEER) indicating that fibronectin supports tight junction formation and barrier function.[72] These observations are interesting since the expression and distribution of cell-cell adhesion proteins is impaired in CCMs.[28,64,73] The endothelial spheroid formation assay which was first described in 1998 is a versatile tool to study EC function in a 3D microenvironment.[74] EC aggregation, organization, and differentiation to a two-compartment system of an unorganized center and a highly organized surface can be analyzed in this model.[74] Not only cell-cell but also cell-matrix interactions play important roles in this organization process. Notably, fibronectin fibers can be found at the periphery of endothelial spheroids.[75] Long-term inactivation of CCM1, CCM2 or CCM3 impairs spheroid formation, especially by inhibiting proper assembly of the surface monolayer. Plasma fibronectin supplementation dramatically improved not only the spheroid formation of *CCM3*$^{-/-}$ CI-huVECs and *CCM3*$^{-/-}$ hCMEC/D3 cells, but also of CCM1-, and CCM2-deficient ECs. Since cell-matrix and cell-cell adhesions are known to influence each other,[76] it seems reasonable to hypothesize that fibronectin replacement promotes spheroid formation of CCM1-, CCM2-, and CCM3-deficient ECs not only in a cell-matrix, but also in a cell-cell adhesion-dependent manner.

In CCM mouse models, vascular lesions predominantly develop in the brain and retina. Fibronectin is an essential ECM component of retinal blood vessels, and its endothelial-specific inactivation in mice leads to reduced radial growth, less vessel branching, and more vascular regression events.[77] This phenotype is partially reminiscent of the leaky retinal lesions that can be found in CCM mouse models. In the retinas of *Ccm1*- and *Ccm3*-knockout mice, a dense network of dysfunctional vessels can be observed at the periphery of the vascular plexus.[13,16,78] Furthermore, treatment of aortic explants with a Gly-Arg-Gly-Asp-Ser (GRGDS) peptide, which inhibits the binding of fibronectin to its cognate integrin receptors induced regression of developing microvessels.[79] An altered dispersion of tight junction proteins which are important elements of the blood brain barrier[80] is accompanied by less fibronectin in CCM lesions.[28] In addition, fibronectin may enhance barrier function through its influence on the localization of tight junction proteins.[81] Together, these observations may lead to the hypothesis that disturbance of fibronectin triggers endothelial dysfunction in *Ccm1*- and *Ccm3*-knockout mice.

Taken together, we show that fibronectin was able to rescue a broad spectrum of endothelial alterations that were induced by the disruption of CCM1, CCM2, and CCM3 in human ECs. However, its supplementation neither rescued

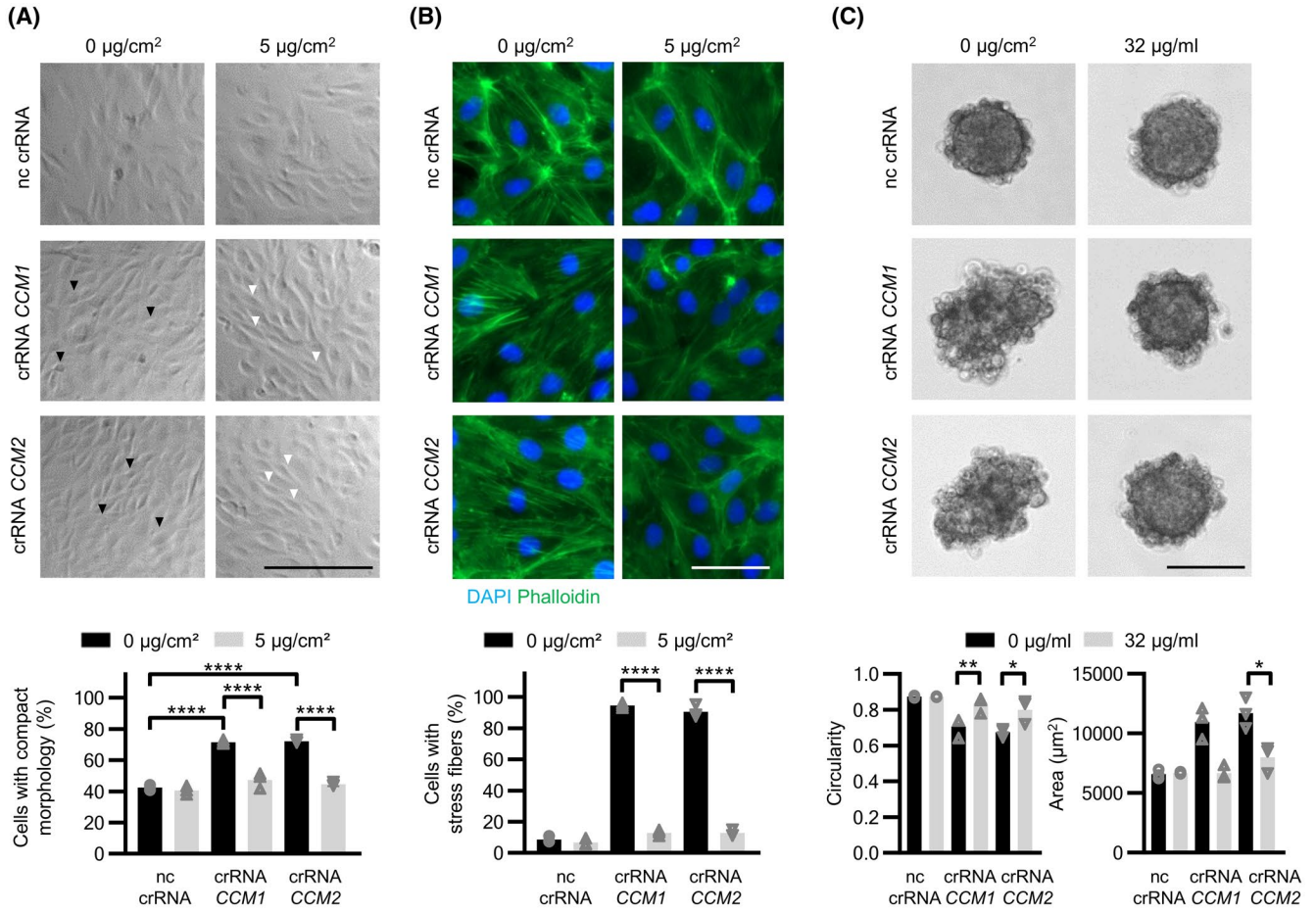

FIGURE 7 Fibronectin replacement attenuates endothelial dysfunction upon CCM1 or CCM2 inactivation in CI-huVECs. A, crRNA:tracrRNA:Cas9 RNP-treated CI-huVECs demonstrated a high proportion of cells with a compact morphology, which was significantly decreased by fibronectin supplementation (1×10^4 cell/well; 96-well plate). Black arrowheads indicate the compact cell shape while white arrowheads indicate cells that regained a spindle-shaped morphology after fibronectin supplementation. Scale bar ≙ 200 µm. B and C, CCM1 and CCM2 inactivation in crRNA:tracrRNA:Cas9 RNP-treated cell mixtures led to an increased stress fiber formation (1×10^4 cells/well; 96-well plate, (B) and an impaired spheroid organization (C), which both were attenuated by fibronectin supplementation. Scale bars ≙ 50 µm (B) and 100 µm (C). crRNA *CCM1* = *CCM1*-targeting RNP, crRNA *CCM2* = *CCM2*-targeting RNP, nc crRNA = non-targeting control RNP. Data are presented as mean and single data points (n = 3). Two-way ANOVA with Holm-Šidák's multiple comparisons test or Student's *t* test were used for statistical analysis: **P* < .05; ***P* < .01; ****P* < .001; *****P* < .0001

aberrant gene expression signatures in *CCM3*$^{-/-}$ ECs nor inhibited their survival advantage. These observations support the conclusion that the formation and progression of CCM lesions are controlled by a complex network of deregulated pathways. A positive influence on individual signaling cascades and endothelial dysfunctions is not necessarily associated with a complete rescue. Therefore, combinatorial strategies are likely required to prevent CCM formation and progression in a therapeutic setting.

ACKNOWLEDGMENTS

Research reported in this publication was supported by the Deutsche Forschungsgemeinschaft (DFG, German Research Foundation) [grant number DFG RA2876/2-2 (MR)] and by the Research Network Molecular Medicine of the University Medicine Greifswald [grant number FOVB-2019-01 (MR)]. P. K. E. Dellweg was supported by a scholarship from the Gerhard Domagk program of the University Medicine Greifswald. We thank R. A. Pilz and D. Skowronek for their excellent technical help in CRISPR/Cas9 off-target site analyzes.

CONFLICT OF INTEREST

The authors declare no conflicts of interest.

AUTHOR CONTRIBUTIONS

K. Schwefel, S. Spiegler, C.D. Much, and P.K.E. Dellweg performed most of the experiments; K. Schwefel, B. C. Kirchmaier, U. Felbor, and M. Rath contributed to the intellectual conception and the design of the study; M. Rath, K. Riedel, and U. Felbor supervised the experiments; K. Schwefel, S. Spiegler, P.K.E. Dellweg, B.C. Kirchmaier,

T. M. Strom, and M. Rath analyzed the data; K. Schwefel, S. Spiegler, P.K.E. Dellweg, and J. Pané-Farré performed the microscopy experiments; all authors contributed to interpretation of the results; K. Schwefel, U. Felbor, and M. Rath drafted the manuscript and all authors contributed to writing.

DATA AVAILABILITY STATEMENT

All relevant data are published within the paper and its supporting additional files.

REFERENCES

1. Gil-Nagel A, Wilcox KJ, Stewart JM, Anderson VE, Leppik IE, Rich SS. Familial cerebral cavernous angioma: clinical analysis of a family and phenotypic classification. *Epilepsy Res*. 1995;21:27-36.
2. Marchuk DA, Srinivasan S, Squire TL, Zawistowski JS. Vascular morphogenesis: tales of two syndromes. *Hum Mol Genet*. 2003;12(Spec No 1), R97-R112.
3. Günel M, Awad IA, Anson J, Lifton RP. Mapping a gene causing cerebral cavernous malformation to 7q11.2-q21. *Proc Natl Acad Sci U S A*. 1995;92:6620-6624.
4. Whitehead KJ, Plummer NW, Adams JA, Marchuk DA, Li DY. Ccm1 is required for arterial morphogenesis: implications for the etiology of human cavernous malformations. *Development*. 2004;131:1437-1448.
5. Laberge-le Couteulx S, Jung HH, Labauge P, et al. Truncating mutations in *CCM1*, encoding KRIT1, cause hereditary cavernous angiomas. *Nat Genet*. 1999;23:189-193.
6. Sahoo T, Johnson EW, Thomas JW, et al. Mutations in the gene encoding KRIT1, a Krev-1/rap1a binding protein, cause cerebral cavernous malformations (CCM1). *Hum Mol Genet*. 1999;8:2325-2333.
7. Liquori CL, Berg MJ, Siegel AM, et al. Mutations in a gene encoding a novel protein containing a phosphotyrosine-binding domain cause type 2 cerebral cavernous malformations. *Am J Hum Genet*. 2003;73:1459-1464.
8. Denier C, Goutagny S, Labauge P, et al. Mutations within the *MGC4607* gene cause cerebral cavernous malformations. *Am J Hum Genet*. 2004;74:326-337.
9. Bergametti F, Denier C, Labauge P, et al. Mutations within the *programmed cell death 10* gene cause cerebral cavernous malformations. *Am J Hum Genet*. 2005;76:42-51.
10. Spiegler S, Rath M, Paperlein C, Felbor U. Cerebral Cavernous Malformations: An Update On Prevalence, Molecular Genetic Analyses, And Genetic Counselling. *Mol Syndromol*. 2018;9:60-69.
11. Cigoli MS, Avemaria F, De Benedetti S, et al. *PDCD10* gene mutations in multiple cerebral cavernous malformations. *PLoS ONE*. 2014;9:e110438.
12. Draheim KM, Fisher OS, Boggon TJ, Calderwood DA. Cerebral cavernous malformation proteins at a glance. *J Cell Sci*. 2014;127:701-707.
13. Zhou HJ, Qin L, Zhang H, et al. Endothelial exocytosis of angiopoietin-2 resulting from CCM3 deficiency contributes to cerebral cavernous malformation. *Nat Med*. 2016;22:1033-1042.
14. Zhou Z, Tang AT, Wong WY, et al. Cerebral cavernous malformations arise from endothelial gain of MEKK3-KLF2/4 signalling. *Nature*. 2016;532:122-126.
15. Zhou Z, Rawnsley DR, Goddard LM, et al. The cerebral cavernous malformation pathway controls cardiac development via regulation of endocardial MEKK3 signaling and KLF expression. *Dev Cell*. 2015;32:168-180.
16. Cuttano R, Rudini N, Bravi L, et al. KLF4 is a key determinant in the development and progression of cerebral cavernous malformations. *EMBO Mol Med*. 2016;8:6-24.
17. Renz M, Otten C, Faurobert E, et al. Regulation of beta1 integrin-Klf2-mediated angiogenesis by CCM proteins. *Dev Cell*. 2015;32:181-190.
18. Detter MR, Snellings DA, Marchuk DA. Cerebral cavernous malformations develop through clonal expansion of mutant endothelial cells. *Circ Res*. 2018;123:1143-1151.
19. Malinverno M, Maderna C, Abu Taha A, et al. Endothelial cell clonal expansion in the development of cerebral cavernous malformations. *Nat Commun*. 2019;10:2761.
20. Schwefel K, Spiegler S, Ameling S, et al. Biallelic *CCM3* mutations cause a clonogenic survival advantage and endothelial cell stiffening. *J Cell Mol Med*. 2019;23:1771-1783.
21. Davis GE, Senger DR. Endothelial extracellular matrix: biosynthesis, remodeling, and functions during vascular morphogenesis and neovessel stabilization. *Circ Res*. 2005;97:1093-1107.
22. Perruzzi CA, de Fougerolles AR, Koteliansky VE, Whelan MC, Westlin WF, Senger DR. Functional overlap and cooperativity among alphav and beta1 integrin subfamilies during skin angiogenesis. *J Invest Dermatol*. 2003;120:1100-1109.
23. Senger DR, Perruzzi CA. Cell migration promoted by a potent GRGDS-containing thrombin-cleavage fragment of osteopontin. *Biochim Biophys Acta*. 1996;1314:13-24.
24. Lopez-Ramirez MA, Fonseca G, Zeineddine HA, et al. Thrombospondin1 (TSP1) replacement prevents cerebral cavernous malformations. *J Exp Med*. 2017;214:3331-3346.
25. Whelan MC, Senger DR. Collagen I initiates endothelial cell morphogenesis by inducing actin polymerization through suppression of cyclic AMP and protein kinase A. *J Biol Chem*. 2003;278:327-334.
26. Liu Y, Senger DR. Matrix-specific activation of Src and Rho initiates capillary morphogenesis of endothelial cells. *FASEB J*. 2004;18:457-468.
27. Kim S, Bell K, Mousa SA, Varner JA. Regulation of angiogenesis in vivo by ligation of integrin alpha5beta1 with the central cell-binding domain of fibronectin. *Am J Pathol*. 2000;156:1345-1362.
28. Schneider H, Errede M, Ulrich NH, Virgintino D, Frei K, Bertalanffy H. Impairment of tight junctions and glucose transport in endothelial cells of human cerebral cavernous malformations. *J Neuropathol Exp Neurol*. 2011;70:417-429.
29. Liu W, Draheim KM, Zhang R, Calderwood DA, Boggon TJ. Mechanism for KRIT1 release of ICAP1-mediated suppression of integrin activation. *Mol Cell*. 2013;49:719-729.
30. Jilkova ZM, Lisowska J, Manet S, et al. CCM proteins control endothelial beta1 integrin dependent response to shear stress. *Biol Open*. 2014;3:1228-1235.
31. Stockton RA, Shenkar R, Awad IA, Ginsberg MH. Cerebral cavernous malformations proteins inhibit Rho kinase to stabilize vascular integrity. *J Exp Med*. 2010;207:881-896.
32. Whitehead KJ, Chan AC, Navankasattusas S, et al. The cerebral cavernous malformation signaling pathway promotes vascular integrity via Rho GTPases. *Nat Med*. 2009;15:177-184.
33. Shenkar R, Shi C, Rebeiz T, et al. Exceptional aggressiveness of cerebral cavernous malformation disease associated with *PDCD10* mutations. *Genet Med*. 2015;17:188-196.
34. Lampugnani MG, Orsenigo F, Rudini N, et al. CCM1 regulates vascular-lumen organization by inducing endothelial polarity. *J Cell Sci*. 2010;123:1073-1080.

35. Stamatovic SM, Sladojevic N, Keep RF, Andjelkovic AV. PDCD10 (CCM3) regulates brain endothelial barrier integrity in cerebral cavernous malformation type 3: role of CCM3-ERK1/2-cortactin cross-talk. *Acta Neuropathol*. 2015;130:731-750.
36. Stemmer M, Thumberger T, Del Sol Keyer M, Wittbrodt J, Mateo JL. CCTop: an intuitive, flexible and reliable CRISPR/Cas9 Target Prediction Tool. *PLoS ONE*. 2015;10:e0124633.
37. Anders S, Pyl PT, Huber W. HTSeq–a Python framework to work with high-throughput sequencing data. *Bioinformatics*. 2015;31:166-169.
38. Love MI, Huber W, Anders S. Moderated estimation of fold change and dispersion for RNA-seq data with DESeq2. *Genome Biol*. 2014;15:550.
39. Brenner KA, Corbett SA, Schwarzbauer JE. Regulation of fibronectin matrix assembly by activated Ras in transformed cells. *Oncogene*. 2000;19:3156-3163.
40. Lorenz L, Axnick J, Buschmann T, et al. Mechanosensing by beta1 integrin induces angiocrine signals for liver growth and survival. *Nature*. 2018;562:128-132.
41. Tin A, Li Y, Brody JA, et al. Large-scale whole-exome sequencing association studies identify rare functional variants influencing serum urate levels. *Nat Commun*. 2018;9:4228.
42. Carpentier G, Martinelli M, Courty J, Cascone I. Angiogenesis analyzer for ImageJ. In: *4th ImageJ User and Developer Conference proceedings*, Mondorf-les-Bains, Luxembourg. ISBN: 2-919941-18-6; 2012:198-201.
43. Singh P, Carraher C, Schwarzbauer JE. Assembly of fibronectin extracellular matrix. *Annu Rev Cell Dev Biol*. 2010;26:397-419.
44. Sabbagh MF, Heng JS, Luo C, et al. Transcriptional and epigenomic landscapes of CNS and non-CNS vascular endothelial cells. *eLife*. 2018;7:e36187.
45. Auerbach R, Lewis R, Shinners B, Kubai L, Akhtar N. Angiogenesis assays: a critical overview. *Clin Chem*. 2003;49:32-40.
46. Draheim KM, Li X, Zhang R, et al. CCM2-CCM3 interaction stabilizes their protein expression and permits endothelial network formation. *J Cell Biol*. 2015;208:987-1001.
47. Borikova AL, Dibble CF, Sciaky N, et al. Rho kinase inhibition rescues the endothelial cell cerebral cavernous malformation phenotype. *J Biol Chem*. 2010;285:11760-11764.
48. Huveneers S, Danen EH. Adhesion signaling-crosstalk between integrins, Src and Rho. *J Cell Sci*. 2009;122:1059-1069.
49. Sarelius IH, Glading AJ. Control of vascular permeability by adhesion molecules. *Tissue Barriers*. 2015;3:e985954.
50. Wu MH. Endothelial focal adhesions and barrier function. *J Physiol*. 2005;569:359-366.
51. Boon RA, Leyen TA, Fontijn RD, et al. KLF2-induced actin shear fibers control both alignment to flow and JNK signaling in vascular endothelium. *Blood*. 2010;115:2533-2542.
52. Wierzbicka-Patynowski I, Schwarzbauer JE. The ins and outs of fibronectin matrix assembly. *J Cell Sci*. 2003;116:3269-3276.
53. Hocking DC, Sottile J, McKeown-Longo PJ. Activation of distinct alpha5beta1-mediated signaling pathways by fibronectin's cell adhesion and matrix assembly domains. *J Cell Biol*. 1998;141:241-253.
54. McKeown-Longo PJ, Mosher DF. Interaction of the 70,000-mol-wt amino-terminal fragment of fibronectin with the matrix-assembly receptor of fibroblasts. *J Cell Biol*. 1985;100:364-374.
55. Spiegler S, Rath M, Much CD, Sendtner BS, Felbor U. Precise *CCM1* gene correction and inactivation in patient-derived endothelial cells: modeling Knudson's two-hit hypothesis in vitro. *Mol Genet Genomic*. 2019;Med:e755.
56. Castro M, Lavina B, Ando K, et al. CDC42 deletion elicits cerebral vascular malformations via increased MEKK3-dependent KLF4 expression. *Circ Res*. 2019;124:1240-1252.
57. Fischer A, Zalvide J, Faurobert E, Albiges-Rizo C, Tournier-Lasserve E. Cerebral cavernous malformations: from *CCM* genes to endothelial cell homeostasis. *Trends Mol Med*. 2013;19:302-308.
58. Wei S, Li Y, Polster SP, Weber CR, Awad IA, Shen L. Cerebral cavernous malformation proteins in barrier maintenance and regulation. *Int J Mol Sci*. 2020;21:675.
59. Goudreault M, D'Ambrosio LM, Kean MJ, et al. A PP2A phosphatase high density interaction network identifies a novel striatin-interacting phosphatase and kinase complex linked to the cerebral cavernous malformation 3 (CCM3) protein. *Mol Cell Proteomics*. 2009;8:157-171.
60. Yoruk B, Gillers BS, Chi NC, Scott IC. Ccm3 functions in a manner distinct from Ccm1 and Ccm2 in a zebrafish model of CCM vascular disease. *Dev Biol*. 2012;362:121-131.
61. Fidalgo M, Fraile M, Pires A, Force T, Pombo C, Zalvide J. CCM3/PDCD10 stabilizes GCKIII proteins to promote Golgi assembly and cell orientation. *J Cell Sci*. 2010;123:1274-1284.
62. Voss K, Stahl S, Schleider E, et al. CCM3 interacts with CCM2 indicating common pathogenesis for cerebral cavernous malformations. *Neurogenetics*. 2007;8:249-256.
63. Stahl S, Gaetzner S, Voss K, et al. Novel *CCM1*, *CCM2*, and *CCM3* mutations in patients with cerebral cavernous malformations: in-frame deletion in CCM2 prevents formation of a CCM1/CCM2/CCM3 protein complex. *Hum Mutat*. 2008;29:709-717.
64. Glading A, Han J, Stockton RA, Ginsberg MH. KRIT-1/CCM1 is a Rap1 effector that regulates endothelial cell cell junctions. *J Cell Biol*. 2007;179:247-254.
65. Faurobert E, Rome C, Lisowska J, et al. CCM1-ICAP-1 complex controls beta1 integrin-dependent endothelial contractility and fibronectin remodeling. *J Cell Biol*. 2013;202:545-561.
66. Otten C, Knox J, Boulday G, et al. Systematic pharmacological screens uncover novel pathways involved in cerebral cavernous malformations. *EMBO Mol Med*. 2018;10.
67. Sun Z, Guo SS, Fässler R. Integrin-mediated mechanotransduction. *J Cell Biol*. 2016;215:445-456.
68. Jansen KA, Atherton P, Ballestrem C. Mechanotransduction at the cell-matrix interface. *Semin Cell Dev Biol*. 2017;71:75-83.
69. Huveneers S, Truong H, Fassler R, Sonnenberg A, Danen EH. Binding of soluble fibronectin to integrin alpha5 beta1-link to focal adhesion redistribution and contractile shape. *J Cell Sci*. 2008;121:2452-2462.
70. Burridge K, Wittchen ES. The tension mounts: stress fibers as force-generating mechanotransducers. *J Cell Biol*. 2013;200:9-19.
71. Cseh B, Fernandez-Sauze S, Grall D, Schaub S, Doma E, Van Obberghen-Schilling E. Autocrine fibronectin directs matrix assembly and crosstalk between cell-matrix and cell-cell adhesion in vascular endothelial cells. *J Cell Sci*. 2010;123:3989-3999.
72. Tilling T, Korte D, Hoheisel D, Galla HJ. Basement membrane proteins influence brain capillary endothelial barrier function in vitro. *J Neurochem*. 1998;71:1151-1157.
73. Boulday G, Rudini N, Maddaluno L, et al. Developmental timing of CCM2 loss influences cerebral cavernous malformations in mice. *J Exp Med*. 2011;208:1835-1847.
74. Korff T, Augustin HG. Integration of endothelial cells in multicellular spheroids prevents apoptosis and induces differentiation. *J Cell Biol*. 1998;143:1341-1352.

75. Bauman E, Feijao T, Carvalho DTO, Granja PL, Barrias CC. Xeno-free pre-vascularized spheroids for therapeutic applications. *Sci Rep*. 2018;8:230.
76. Weber GF, Bjerke MA, DeSimone DW. Integrins and cadherins join forces to form adhesive networks. *J Cell Sci*. 2011;124:1183-1193.
77. Turner CJ, Badu-Nkansah K, Hynes RO. Endothelium-derived fibronectin regulates neonatal vascular morphogenesis in an autocrine fashion. *Angiogenesis*. 2017;20:519-531.
78. Maddaluno L, Rudini N, Cuttano R, et al. EndMT contributes to the onset and progression of cerebral cavernous malformations. *Nature*. 2013;498:492-496.
79. Nicosia RF, Bonanno E, Smith M. Fibronectin promotes the elongation of microvessels during angiogenesis in vitro. *J Cell Physiol*. 1993;154:654-661.
80. Liu WY, Wang ZB, Zhang LC, Wei X, Li L. Tight junction in blood-brain barrier: an overview of structure, regulation, and regulator substances. *CNS Neurosci Ther*. 2012;18:609-615.
81. Koval M, Ward C, Findley MK, Roser-Page S, Helms MN, Roman J. Extracellular matrix influences alveolar epithelial claudin expression and barrier function. *Am J Respir Cell Mol Biol*. 2010;42:172-180.

SUPPORTING INFORMATION

Additional Supporting Information may be found online in the Supporting Information section.

How to cite this article: Schwefel K, Spiegler S, Kirchmaier BC, et al. Fibronectin rescues aberrant phenotype of endothelial cells lacking either CCM1, CCM2 or CCM3. *The FASEB Journal*. 2020;00:1–16. https://doi.org/10.1096/fj.201902888R